Discharge constriction, photodetachment, and ionization instabilities in electron-beam-sustained discharge excimer lasers[a)]

M. J. Kushner[b)] and A. L. Pindroh
Spectra Technology Inc. (Formerly Mathematical Sciences Northwest), 2755 Northup Way, Bellevue, Washington 98004

(Received 26 February 1986; accepted for publication 24 April 1986)

Rare gas–halogen excimer lasers excited by electron-beam-sustained discharges (EBSD) will operate stably for only a limited length of time (hundreds of nanoseconds to a few microseconds). In this paper, results from a multidimensional model for an EBSD KrF laser are used to study various aspects of discharge ionization and geometric stability, and the relationship between the two. We examine the effects of photodetachment of electrons from the halogen negative ion, of circuit response, and of nonuniform *e*-beam power deposition upon the onset of discharge instabilities. We find that both spontaneous emission from KrF^* and laser oscillation resulting in photodetachment of electrons from F^- can initiate an ionization instability. By operating with high impedance electrical circuits, the tendency towards instabilities by this effect can be reduced. We also find that the spatial uniformity of the *e*-beam power deposition is directly correlated with both the rate of discharge constriction and the time at which the discharge suffers an ionization instability.

I. INTRODUCTION

Rare gas–halide lasers excited by electron-beam (*e*-beam) sustained discharges have long held the promise of higher overall efficiency than the *e*-beam excited variants of these lasers. A major consideration in scaling *e*-beam sustained discharge lasers to higher power is discharge stability, an issue that has been a significant topic of both theoretical and experimental studies.[1–10] To extend the results of these prior works, we have performed a theoretical study of KrF *e*-beam sustained discharge (EBSD) lasers including geometrical effects not previously treated in detail. The purpose of this work is to determine whether a more careful control of certain parameters such as circuit values and the uniformity of *e*-beam power deposition can improve the performance of EBSD KrF lasers. The KrF laser was chosen for this study because of its demonstrated high efficiency which makes it a viable candidate as an inertial confinement fusion laser when combined with various optical pulse compression techniques.

In a stable discharge, the average electron density and discharge current reach quasi-steady-state values, and the spatial distribution of power deposition reaches a quasi-steady-state distribution. An instability which causes the quasi-steady-state electron density and current to initiate an exponential growth is called an ionization instability. An instability resulting in a geometric change in the distribution of power deposition in the discharge is called discharge constriction or collapse. In this paper, the effect of photodetachment and circuit response on ionization instabilities and the effect of nonuniform *e*-beam power deposition on the ionization stability and constriction of large aperture EBSD lasers are examined. This study is performed with results from a two-dimensional, time-dependent model for a KrF EBSD laser.

In brief summary, we found that discharge stability and constriction are not particularly sensitive to *e*-beam power deposition that is not uniform in the longitudinal direction; that is, in the direction of the applied electric field. Nonuniform power deposition in this direction tends to be self-correcting due to redistribution of the local electric field. Discharge stability and constriction are, though, sensitive to *e*-beam power deposition that is not uniform in the transverse direction; that is, in the direction perpendicular to the applied electric field. These conclusions are consistent with the theories of Long[6] and Haas.[8] We found that two other effects are also important considerations for discharge stability: response of the discharge circuit and photodetachment of electrons from negative ions. The former effect, noted by Long,[6] has two limiting extremes: low-impedance circuits which appear as constant voltage sources (i.e., constant E/N) and high-impedance circuits which appear as constant sources of current. The latter effect, photodetachment, has not been previously examined in detail. Under certain conditions, the increase in photodetachment at laser threshold can initiate a discharge ionization instability and increase the rate of discharge constriction.

We discuss results for two KrF *e*-beam sustained discharges both having gas mixtures of $Ar/Kr/F_2 = 94.5/5.0/0.5$. The first is a small aperture discharge having dimensions which approximate the experiments of Brown and Nighan.[4] The second is a large aperture discharge whose dimensions are consistent with a KrF laser capable of delivering many hundreds of joules of optical energy ($\lambda = 248$ nm). The large aperture discharge also approximates the experiments of Lacina and Cohn.[11]

Although the discussion here is specific to *e*-beam sustained discharge KrF lasers, the general conclusions apply to EBSD excimer lasers in general. The modeling techniques are also directly applicable to self-sustained discharge excimer lasers. This is accomplished by replacing, in the mod-

[a)] This work was supported by Los Alamos National Laboratory, Contract No. 9-X65-W1478-1.
[b)] Present address: Universtiy of Illinois, 607 E. Healey, Champaign, Illinois 61820.

 0021-8979/86/150904-11$02.40

el, the time and spatially dependent source of ionization by the e beam with the source of (pre)ionization by XUV or x rays typically used for self-sustained discharges.

An overview discussion on discharge stability is given in Sec. II. The discharge model is described in Sec. III. In Sec. IV, the effects of photodetachment and circuit response on discharge ionization stability are discussed. The effects of nonuniform e-beam power deposition on discharge stability are discussed in Sec. V. Concluding remarks are in Sec. VI.

II. GENERAL DISCUSSION ON DISCHARGE STABILITY

The origin of the ionization instability can be simply seen from the following brief analysis. Assume that the gas in the discharge can be represented by a three-level atomic system. (See Fig. 1.) Conservation equations for the electron density and the density of the excited state are

$$\frac{dn_e}{dt} = n_e r_{0I} N_0 + n_e r_{1I} N_1 - (n_e r_a N_a - \beta_d) + S_e, \quad (1)$$

$$\frac{dN_1}{dt} = n_e (r_{01} N_0 - r_{1I} N_1) - \frac{N_1}{\tau} + S_1, \quad (2)$$

where n_e is the electron density, N_j is the density of level j, r_{ij} is the electron impact rate constant between levels i and j (I is for the ion), r_a is the rate constant for attachment, and N_a is the density of the halogen donor. The rate of detachment is β_d, the lifetime of the excited state is τ, S_e is a source of ionization which is independent of the bulk electron density (i.e., the e beam), and S_1 is the analogous term for the excited state. Assuming quasi-steady-state conditions for N_1, one obtains

$$\frac{dn_e}{dt} = n_e (N_0 r_{0I} + S_1 \tau r_{1I}) + n_e^2 r_{10} r_{1I} N_0 \tau - n_e r_a^* N_a + S_e, \quad (3)$$

where $r_a^* = r_a - \beta_d/(n_e N_a)$ represents the net attachment rate (attachment—detachment). The first and third terms of Eq. (3) are linear in n_e. Ignoring for the moment S_e, a stable nonexponentially increasing solution can be obtained for the electron density as long as the second term, representing multistep ionization from the excited state and proportional to n_e^2, is small compared to the linear terms. An instability is initiated when the second term of Eq. (3) begins to dominate either as a result of an increase in multistep ionization or a decrease in attachment. This mechanism for initiating an ionization instability in excimer discharges was first suggested by Daugherty *et al.*[1] They identified two step ionization from the metastable levels of Kr (denoted Kr*) as the source of instability in KrF excimer lasers.

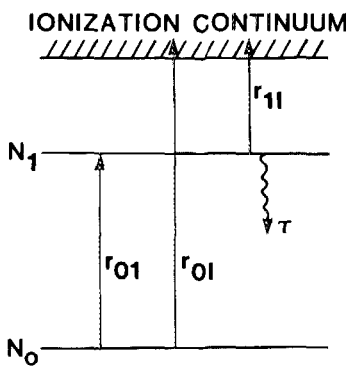

FIG. 1. Model three-level system for discharge ionization stability analysis.

The product of $r_{01} r_{1I}$ is an exponentially increasing function of the normalized applied electric field E/N (electric field/gas number density) for the region of interest (E/N = 5–20 Td, 1 Td = 10^{-17} V cm^{-2}). Stability in typical excimer discharges can be obtained for extended periods of time (many hundreds of ns) by keeping this product small; that is, by operating at low values of E/N ($<$ 10–15 Td). Under these conditions, though, the rate of attachment exceeds the rate of ionization. The discharge must then be sustained by providing a source of ionization S_e which is independent of the bulk electron density. This is the principle of the electron-beam sustained discharge excimer laser[1,6,10–12] in which an electron beam is injected into the discharge (usually through the cathode) to provide the external source of ionization. In general, stable discharge excimer lasers are limited to power deposition of a few hundred kW cm^{-3} for a few hundred ns before an ionization instability develops.

A figure of merit for EBSDs is the discharge enhancement, $\eta = P_D/P_{EB}$, where P_D is the total power deposited by the discharge and P_{EB} is the power deposited by the e beam.[1,3,5,6] Due to losses associated with the penetration of the e beam through foils and the cathode, the efficiency with which power is deposited in the gas by the e beam is less than that for the discharge. One therefore desires to operate at large values of η for high efficiency, yet at low values of η (i.e., low values of E/N) to insure stability. Daugherty *et al.*[1] and Rokni *et al.*[3] concluded that EBSDs can operate with large discharge enhancement factors $\eta > 5$ and with a high efficiency (70%–80%) for creating Kr metastables (the precursor to the upper laser level). These large values of η, though, can only be obtained by lowering the absolute power deposition in the discharge. Long[6] determined that the maximum permissible stable values of power deposition are related $P_D^{\max} \propto P_{EB}^{0.3}$, so $\eta \propto P_{EB}^{-0.7}$. This relationship is valid provided that the e-beam power deposition is spatially uniform. Brown and Nighan[4] and Nighan[5] also concluded that there appears to be limiting value of η for which discharges will remain stable after observing in their experiments that the time for stability decreased as E/N, and hence η, increased.

The probability that a discharge suffers an ionization instability can increase if the power deposition, by either the e beam or subsequently by the discharge itself, is not uniform. Conceptually, the discharge can be modeled as a set of parallel resistors in the direction of the applied electric field. The resistance of each element in the array is approximately inversely proportional to the local power deposition. A nonuniformity in the plasma causing one of the resistors to become more conductive is inherently unstable since the more conductive resistor will draw more power and become even more conductive. This condition eventually leads to geometrical constriction of the discharge. In a previous study, we showed that self-sustained discharge lasers are quite susceptible to constriction when power deposition is not uniform.[13] In analogy EBSDs can also be expected to be susceptible to instabilities when power deposition is not uniform.[6,8]

The relationship between discharge constriction and ionization instability has been qualitatively made. Brown and Nighan[4] noted that one or more large volume arcs (≈ 1 cm wide) were present in their EBSD whenever an ionization instability occurred. Rokni *et al.*[3] also experimentally observed that the onset of an ionization instability is preceded by, or coincident to, the onset of discharge constriction. These observations correlate with the theory of Haas[8] which states that discharges are unstable with respect to perturbations with transverse wavevectors.

To first order, the parameter E/N and the relative density of components in the gas mixture determine the electron impact excitation rate coefficients in an EBSD and hence determine the time for onset of an ionization instability.[14] Other parameters may also be important, in particular f_m, the fraction of krypton (Kr*) or argon (Ar*) metastables, and f_e, the fractional electron density. When f_m is large ($\geqslant 10^{-5}$),the rate of excitation of Kr* decreases due to a reduction in the high energy tail of the electron distribution.[2,5] Long[15] found that the transition to a Maxwellian-like electron distribution function when $f_e > 10^{-7}$ increases the rate at which Kr* and Ar* are excited. To the extent that ionization instabilities in KrF EBSDs result from multistep ionization from Kr* and Ar*, f_m and f_e are important parameters in determining discharge stability.

III. DESCRIPTION OF THE MODEL

Kinetics models[16] for discharge[1-7,9,11,14,15,17] and *e*-beam[3,18-23] pumped KrF lasers have matured through the years. The model developed for this study builds upon these previous works but differs from them in that it extends the analysis to multiple spatial dimensions. The model simulates, in two dimensions and time, an *e*-beam sustained discharge in a gas mixture of $Ar/Kr/F_2$. The plane of interest is parallel to the applied electric field and perpendicular to the plane of the transverse electrodes and the optical axis (See Fig. 2.) The model is comprised of a self-consistent accounting of electron collision kinetics, heavy particle kinetics, the driving electrical circuit, *e*-beam power deposition, and, when operating as an oscillator, optical gain and absorption of the laser flux. The species included in the model are listed in Table I.

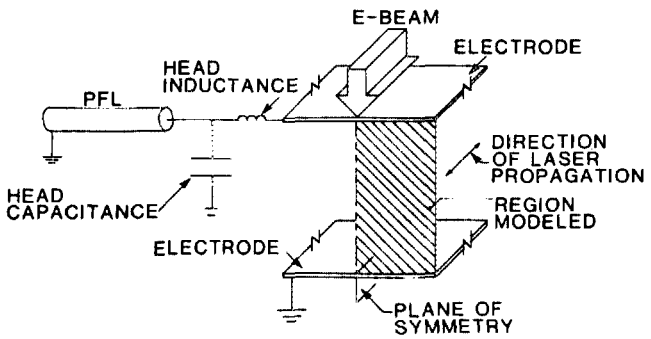

FIG. 2. Schematic of the large aperture *e*-beam sustained discharge laser. The transverse dimensions are 18 cm × 18 cm. The electrode length is 75 cm. The *e* beam is incident through the upper (cathode) electrode. The mechanical body of the discharge is electrically represented by the laser head inductance and head capacitance. The discharge is driven by a pulse forming line (PFL) of specified impedance and electrical length. The two-dimensional model simulates values in the indicated space which is symmetric across the midplane of the discharge.

The following conceptual sequence of operations is used to advance a single time step in the model. To begin, the *e*-beam power deposition, $P_{EB}(x,y,t)$, is specified on a rectangular computational mesh as a function of time and position in the discharge. The value of $P_{EB}(x,y,t)$ specifies the local rate of ionization and excitation by beam electrons. Rate constants for bulk (i.e., not *e* beam) electron impact collisions are obtained from the local value of the electric field and other plasma parameters. These rate constants, and those for heavy particle collisions, are used as input to a system of rate equations for each spatial grid point in the plane of interest. We assume that the discharge is symmetric across the midplane of the discharge (see Fig. 2). Therefore, the computational mesh overlays only half of the discharge. The rate equations are advanced in time using a third order Runga–Kutta integration scheme. Based on the local values of conductivity in the plasma $\sigma(x,y,t)$ the effective resistance of the discharge is computed and used as input to a set of rate equations for the external circuit, which is then advanced the desired time step. The revised voltage drop across the plasma is then used for boundary conditions for a solution of a modified Laplace's equation which yields the local value of the electric potential and, by differentiation, the electric field $E(x,y,t)$. The local value of the electric field and other local plasma parameters are then used to obtain the electron impact rate coefficients, thereby completing the integration time step.

The kinetics portion of the model is conceptually similar to other recently published models for KrF lasers (see above) and the discharge circuit model is similar to that in a recently published analysis of the HgBr avalanche discharge laser.[13] Therefore, these topics will be only briefly discussed.

A. *e*-beam, electron impact, and heavy particle kinetics

The *e*-beam, electron impact, and heavy particle reactions included in the model differ little from those used by Kannari *et al.*[23] in their model for an *e*-beam pumped KrF laser. The reader is therefore referred to their work for a list of the reactions and heavy particle rate constants. A detailed listing of the reactions, rate constants, and source for cross sections used in this study can be found in Ref. 24 or can be obtained by request from the authors. The major difference between the reactions included by Kannari *et al.* and those used here is that electron impact processes with F_2 (e.g., vibrational and electronic excitation, and ionization) were

TABLE I. Species included in the model.

Ar	Ar* (4*s*)	Ar** (4*p*)	Ar^+
Kr	Kr* (5*s*)	Kr** (5*p*)	Kr^+
Ar_2^*	Ar_2^+	Kr_2^*	Kr_2^+
ArF*	KrF*	Ar_2F^*	Kr_2F^*
ArKr*	$ArKr^+$	ArKrF*	
F_2	$F_2^*(a^3\Pi, A\,^1\Pi_u)$	$F_2^{**}(C\,^1\Sigma_u^+, H\,^1\Pi_u)$	F_2^+
F	F^-		
e (bulk electrons)	*e** (*e*-beam electrons)		
ϕ (laser flux 248 nm)	T_g (gas temperature)		

included both in the kinetics and in the solution of Boltzmann's equation for the electron distribution function. By including these additional processes, gas mixtures having high fractions of F_2 (>0.01) can be studied. The cross sections for F_2 were obtained from Hayashi and Nimura.[25]

Local e-beam power deposition $P_{EB}(x,y,t)$ is treated as a parameter in this study. That is, we specify the form of $P_{EB}(x,y,t)$ in order to determine the sensitivity of other discharge parameters on its form. The local rates of ionization and excitation by the e beam are given by their appropriate W values (energy/ion pair). The rate of excitation of the metastable states of Kr and Ar was assumed to have a rate 0.24 that of ionization.

The local values of the bulk electron impact rate constants are calculated by convolving the appropriate cross section with the electron distribution function for the local values of E/N. The electron distribution function is obtained by solving Boltzmann's equation using the program developed by Morgan which is described in Ref. 26. The electron distribution function was parameterized as a function of E/N, gas mixture, f_e, and f_m. The resulting electron impact rate constants were entered into a look-up table which was interpolated during execution of the model. A representative selection of electron impact rate constants and effective electron temperature appears in Fig. 3.

B. Solution for the local electric field

One of the more important processes, with respect to discharge stability, which occurs in a EBSD is the local variation of the applied electric field resulting from the plasma conductivity not being uniform. Since conduction current j must be conserved (and ignoring displacement current) the local electric field can be obtained by solution of

$$\nabla \cdot j = \nabla \cdot \sigma E = -\nabla \cdot \sigma \nabla \Phi, \tag{4}$$

where Φ is the local electric potential. Equation (4) is a valid solution for the electric potential provided that the penetration time for the electric field into the plasma is short compared to the time scale of interest. A diffusion time for the penetration of the electric field τ_p can be approximated by $(\mu_0 \sigma L^2)/\pi^2$ where L is the transverse dimension of the plasma.[27] For our conditions, $\sigma \approx 10^{-2}\ \Omega^{-1}\ \text{cm}^{-1}$ and $L < 10$ cm. Therefore, $\tau_p \approx 1.5$ ns which is much less than the characteristic time over which the applied electric field changes (≈ 10 ns).

The method of successive over relaxation[28] (SOR) was used to solve Eq. (4). The electrode surfaces were modeled as being flat to minimize the local variation in the electric field between the electrodes resulting from the shape of the electrodes. A ground plane representing the current return path was placed at the exterior boundary of the computational mesh at a distance from the center plane of symmetry approximately equal to 1.5 times the electrode spacing.

C. Circuit model

A full circuit description was included in the model. The circuit model is conceptually similar to that described in Ref. 13. We assumed that the discharge is initiated by turning on the e beam so that the model for the rail-gap switch described in Ref. 13 was not used. The results discussed below use two variations of the circuit model. The first uses only a single capacitor for energy storage while the second uses a PFL (pulse-forming line). Computationally, the PFL is modeled as a ten-stage PFN (pulse-forming network). The single capacitor is modeled in the same fashion; however, only the first stage of the PFN is used.

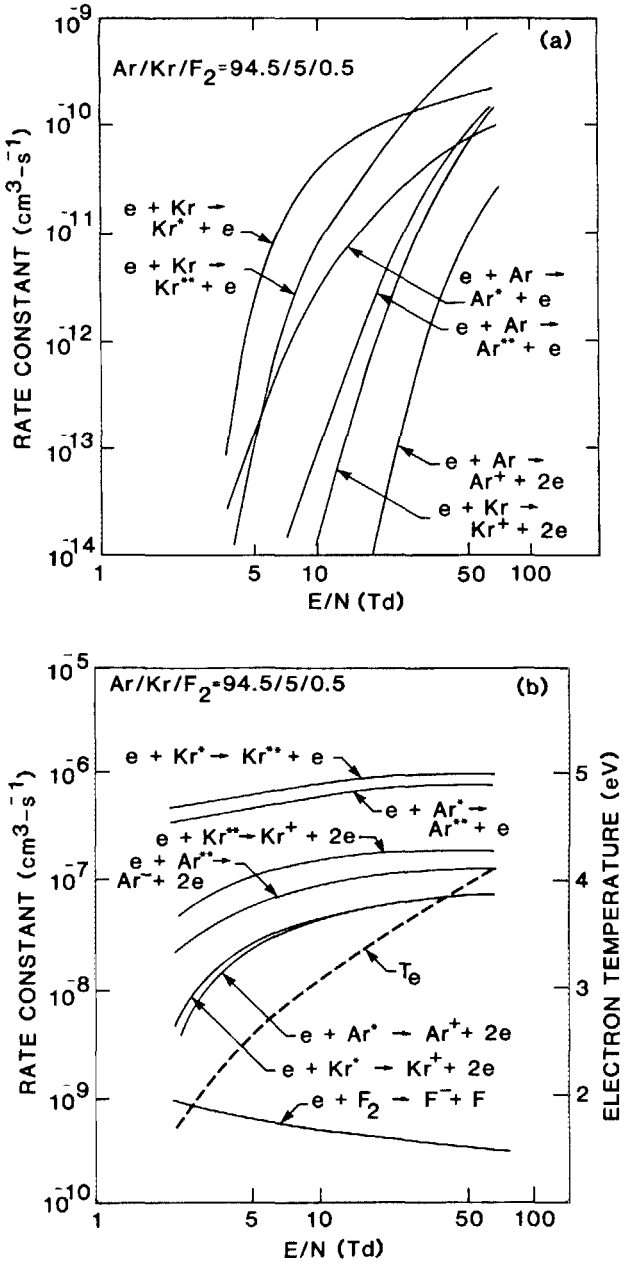

FIG. 3. Representative electron impact rate constants and electron temperature ($T_e = 2\epsilon/3k$, ϵ = average electron energy) as a function of E/N (electric field/number density, 1 Td = 10^{-17} V cm^{-2}). The gas mixture is $Ar/Kr/F_2 = 94.5/5.0/0.5$. (a) Ground state to excited states, as defined in Table I. (b) Excited state collisions, dissociative attachment, and electron temperature.

IV. VOLUMETRIC IONIZATION INSTABILITIES

A. Photodetachment

In this section, the onset of volumetric ionization instabilities is discussed for EBSDs having a gas mixture of Ar/

$Kr/F_2 = 94.5/5/0.5$. By volumetric, we mean that we are excluding the effect of nonuniform power deposition by the e beam. The selected conditions approximate the experiments of Brown and Nighan.[4] The discharge aperture is 2 cm × 2 cm and the discharge length is 45 cm. The volume average e-beam power deposition is 20 kW cm^{-3}. The discharge circuit consists of a single-capacitor (1 μF) closed coupled (inductance 15 nH) to the discharge electrodes.

The time at which an ionization instability begins for these conditions is plotted in Fig. 4 as a function of E/N at the start of the instability. The ionization instability is indicated by an abrupt increase in discharge current (current "runaway"). Results from our model as well as the experimental and theoretical results of Brown and Nighan[4] are plotted in the figure. Our results for these conditions confirm the conclusions of Brown and Nighan[4,7] that the ionization instability occurs primarily as a result of multistep ionization from Kr* and Ar*, and secondarily from halogen burnup. For the discharges in Fig. 4, the fractional halogen burnup at the time of instability increases from ≈12% at 17 Td to ≈42% at 12 Td. As a result of this burnup, the metastable density when multistep ionization exceeds attachment at 12 Td is only 0.6 that at 17 Td, thereby decreasing the time to instability at the lower value of E/N. The total energy deposited by the discharge (time integral of $V \cdot I$) also increases from ≈40 to ≈120 J/l from 17 to 12 Td (see Fig. 5). More energy is deposited at lower E/N by delaying the onset of the ionization instability. The onset of the ionization instability is therefore not a threshold event determined by depositing some critical amount of energy.

The results of this model, and those of Brown and Nighan,[4] both overpredict the time for which the discharge is stable at low values of E/N (see Fig. 4). Two effects, not included in the theory to this point, appear to the cause. The first, is photodetachment of electrons from F^-. The second, discharge uniformity, will be discussed below. The discharges which are in Fig. 4 were not operated as lasers. Therefore there is not a directed high-intensity flux of photons within the discharge cavity. There is, though, a large random flux of photons resulting from spontaneous emission of the exciplex KrF* ($\lambda = 248$ nm, $h\nu = 5$ eV). These photons have sufficient energy to detach electrons from F^- (electron affinity 3.45 eV). The rate of excitation of KrF* for these conditions is approximately 6×10^{22} cm^{-3} s^{-1} and approximately half of the KrF* is nonradiatively quenched. The random 248-nm photon flux is therefore $\approx 10^{21}$ cm^{-2} s, which when coupled with the photodetachment cross section of F^- of 5.4×10^{-18} cm^{-2}, represents a non-neglible source of free electrons.

The contribution of photodetachment resulting from the spontaneous emission of KrF* was included in the model and the time to instability was calculated. The random flux of photons at 248 nm, ϕ_R, was approximated by including in the model the rate equation

$$\frac{d\phi_R}{dt} = \frac{[\mathrm{KrF}^*]L}{4\tau_r} - \frac{2\phi_R c}{L} - \sum_i \phi_R \sigma_i N_i, \qquad (5)$$

where τ_r is the radiative lifetime of KrF*, σ_i is the photoabsorption cross section of species N_i, and L is the transverse dimension of the discharge. The second term in Eq. (5) is the average rate of escape of photons from the discharge in the transverse direction. These results are also shown in Fig. 4 and show quite good agreement with the experiment, particularly at low values of E/N where the analysis ignoring this effect showed poor agreement. The implication of these results is that large aperture KrF excimer EBSDs are more susceptible to instabilities initiated by photodetachment from spontaneous emission because the average escape time of photons is longer.

The decrease in the time of discharge stability by photodetachment, *for these circuit conditions*, is exacerbated when operating the discharge as a laser. The magnitude of the laser flux that will significantly perturb the stability of the discharge can be estimated from Eq. (3). For the conditions of

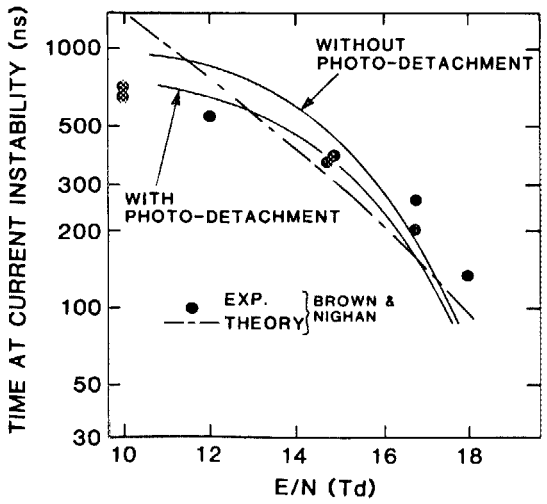

FIG. 4. Time after initiation of the discharge for the onset of an ionization instability as a function of E/N at the time of instability; our model results with the experimental and model results of Brown and Nighan.[4] Two of our cases are shown; with and without photodetachment by spontaneous emission from KrF*.

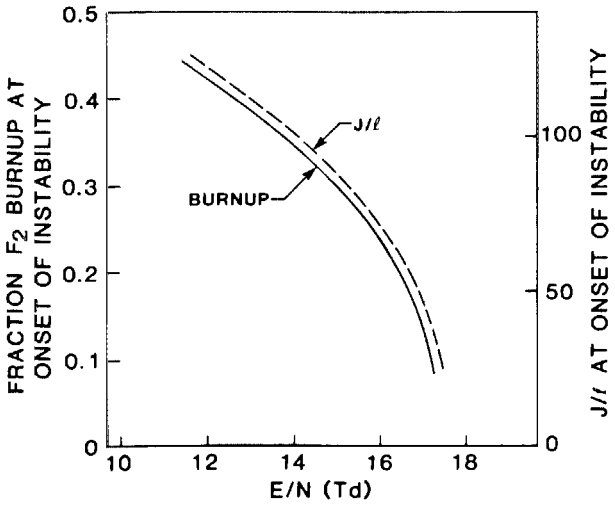

FIG. 5. Fractional burnup of F_2 and discharge energy deposition at the time of onset of an ionization instability for the conditions of Fig. 4. More energy is deposited at lower E/N by extending the period of stability.

Fig. 4 at 15 Td, the contributions to the normalized rate of change in electron density, $(dn_e/dt)/n_e$ ($n_e = 6\times10^{13}$ cm^{-3}) are (units of s^{-1}): e beam, 7.9×10^7; excited state ionization 3.4×10^7; and attachment, 1.1×10^8. The density of F^- is 10^{14} cm^{-3}. The fractional increase in the rate of electron production resulting from photodetachment by the laser flux is therefore $0.1\,\phi$, where the laser flux ϕ has units MW cm^{-2}.

To determine the effect of photodetachment on discharge stability, the time to instability was calculated as a function of the reflectivity of the output mirror R_0 when operating the discharge as a laser. Laser threshold is reached at shorter times and the average intracavity flux is higher with large values of R_0. The time for onset of an ionization instability and the intracavity laser flux at that time are plotted in Fig. 6. An ionization instability is initiated when the intracavity laser flux reaches $\simeq$500 kW cm^{-2} s^{-1} corresponding to a 5% increase in the rate of ionization. (The *maximum* intracavity flux in each case is a few MW/cm^2.) The rate of ionization and electron attachment are equal to within a fraction of a percent prior to laser threshold (that is, dn_e/dt is nonzero and a small fraction positive). The perturbation resulting from photodetachment at laser threshold is, therefore, instantaneously large compared to the quiescent dn_e/dt and is sufficient to initate an ionization instability.

Large excimer lasers usually operate with $R_0 \leqslant 0.3$ and with PFLs having a higher impedance per unit discharge length than that used in above. A low-impedance driver tends to increase the effect of photodetachment on discharge stability due to the rapid response of the discharge circuit. The effect of circuit response on discharge stability is discussed in the next section.

B. Circuit response

Brown and Nighan[4,7] and Long[6] have suggested that another important parameter in determining the stability of discharges is the response of the discharge circuit. Specifically, the parameter of interest is the ability of the circuit to deliver current to the discharge at a sufficiently high rate to sustain the instability. To demonstrate this dependence, we reformulated Eq. (3) by assuming that the rate constants r_{ij} can be written in the vicinity of a preselected operating point of E/N as

$$r_{ij} = r_{ij}^0\left(\frac{E}{N}\right)^{k_{ij}},\quad E = j_0\left(\frac{m_e\nu_m}{n_e e^2}\right)^{\gamma} \propto \left(\frac{1}{n_e}\right)^{\gamma}, \tag{6}$$

where j_0 is the equilibrium current density. The parameter γ represents the degree to which the circuit responds to changes in the plasma conditions. If $\gamma = 1$, then the driving circuit has a high impedance per unit discharge length; that is, the circuit has a large distributed inductance. If the plasma conductivity suddenly changes, the circuit cannot increase or decrease the flow of current fast enough to keep the voltage drop across the plasma a constant and the change in voltage is dropped across the inductance of the circuit. The voltage drop across the plasma is therefore directly proportional to the conductivity of the plasma. If $\gamma = 0$, the discharge circuit has a low impedence per unit discharge length. The circuit has sufficiently low inductance and sufficiently high capacitance that it can supply enough prompt current to maintain a constant voltage drop across the plasma regardless of its conducitivity. We expanded Eq. (3) in the perturbation $n_e \rightarrow n_0(1+\epsilon)$ using Eq. (6) for r_{ij} and E, and kept terms to first order in ϵ. The rate of increase in electron density, $\delta_e = (dn_e/dt)/n_e$, was calculated as a function of γ and ϵ. For simplicity we chose an EBSD in a $Kr/F_2 = 99.5/0.5$ mixture at 1 atm with $E_0/N = 20$ Td and $P_{EB} = 20$ kW cm^{-3}. The response of δ_e to the perturbation ϵ, $d\delta_e/d\epsilon$ is plotted in Fig. 7 as a function of γ for varying values of the fractional electron density f_e. Stable discharges have negative values of $d\delta_e/d\epsilon$; unstable discharges have positive values. We see that for all values of f_e, the higher the impedance of the driving circuit (that is, the larger the value of γ), the more stable the discharge becomes. This trend results from the self-compensating change in E/N and excitation rates which occur when the conductivity of the plasma changes.

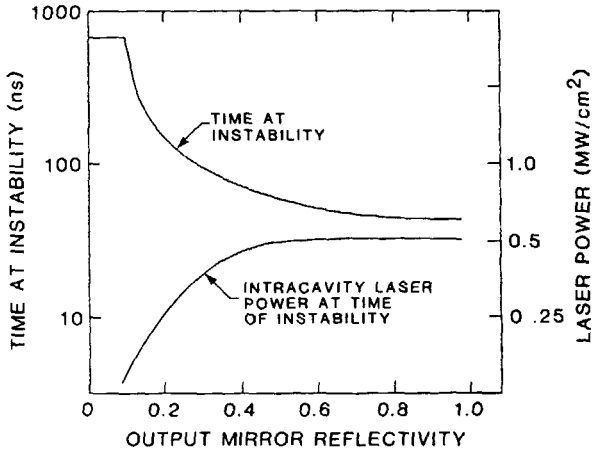

FIG. 6. Time at onset of an ionization instability as a function of output mirror reflectivity when the discharge of Fig. 4 is operated as a laser. The E/N at the time of instability is approximately 15 Td. Also shown is the intracavity laser flux at the time of instability.

A numerical example of the effect of circuit impedance on discharge stability is plotted in Fig. 8. For these results, the single capacitor in the circuit for the previous examples was replaced with a PFL having an electrical length of 2 μs. The head inductance remained 15 nH and the head capacitance was 2 nF. The charging voltage on the PFL was 16 kV (corresponding to 16 Td) and the normalized impedance of the PFL (ohms per unit discharge length for a square aperture) is a parameter. From Fig. 8 we see that for low values of the normalized PFL impedance (small γ), the discharge sustains a high value of E/N and remains stable for only short times. For high values of the normalized PFL impedance (large γ), the delivery of current to the discharge is inductively limited, thereby limiting the operative E/N of the discharge to a value which insures stable operation. Even though the instantaneous power deposition in the discharge is lower when using a higher impedance PFL, more energy is deposited before the ionization stability occurs than for a low impedance PFL because the time for stability is longer.

The tolerance of the discharge to perturbations in the rate of electron production improves with increasing imped-

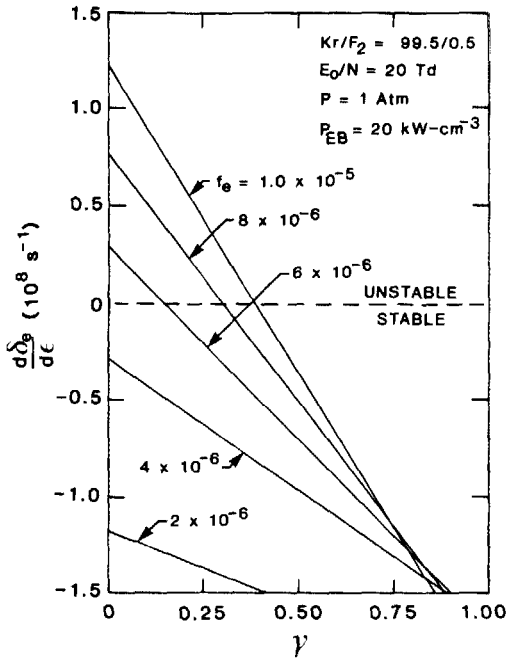

FIG. 7. The sensitivity of the rate of change in electron density δ_e for the perturbation $n_e \rightarrow n_0(1+\epsilon)$ as a function of discharge response γ for different values of the fractional electron density f_e. Small values of γ correspond to low-impedance PFLs; large values of γ correspond to high-impedance PFLs. Unstable discharges have positive values of $d\delta_e/d\epsilon$; stable discharges have negative values. These results are for $Kr/F_2 = 99.5/0.5$, 1 atm, $E_0/N = 20$ Td, and $P_{EB} = 20$ kW cm^{-3}.

ance of the PFL. In particular, the probability of initiating an ionization instability by photodetachment when laser threshold is reached decreases with increasing impedance of the PFL. This trend is shown in Fig. 9 where a mirror reflectivity of 90% was used to accentuate the effect of the photodetachment. For low values of PFL impedance, an ionization instability is triggered when ϕ exceeds 500 kW cm^{-2}. For sufficiently large values of PFL impedance, photodetachment has little effect on discharge stability. The improved tolerance at high impedance results from a decrease in the E/N sustained by the discharge at laser threshold thereby compensating for the source of electrons resulting from photodetachment.

The onset of a volumetrically uniform ionization instability is by itself *not necessarily detrimental* to the performance of the laser. The increase in current at the onset of the instability also increases power deposition. Since the formation efficiency of KrF* remains nearly unchanged until the halogen donor burns up, laser power also increases. The onset of an ionization instability is detrimental to laser performance because the accompanying increase in power deposition initiates other instabilities, primarily geometric in nature, which then degrade laser performance. Some of these instabilities are discussed below.

V. *e*-BEAM UNIFORMITY

The tendency toward constriction in self-sustained discharge lasers is particularly sensitive to spatial nonuniformities in E/N, preionization electron density, and species consumption (e.g., halogen burnup) because the distribution of power deposition is totally determined by the relative conductivity of the plasma, which is in turn a function of the local power deposition.[13] In EBSDs a fraction $(1/\eta)$ of the power deposition is provided by the e beam and is independent of the discharge current. Therefore the local plasma conductivity will not decrease below a minimum value set by the e beam. Spatial differences in plasma conductivity are consequently smaller in EBSDs than in self-sustained discharges and the tendency toward constriction is less. Nevertheless, the uniformity of the power deposited by the e beam is an important parameter in determining the degree of constriction of the discharge and in determining the ionization stability of an EBSD.

In this section we discuss the effect of nonuniform e-beam power deposition on the ionization stability and constriction of the discharge. In this discussion, we use the large aperture laser shown schematically in Fig. 2. The discharge aperture is 18 cm × 18 cm and the discharge length is 75 cm. The gas pressure is 1.5 atm, the PFL has an impedance of 2.7 Ω/m, and the charging voltage of the PFL in 100 kV (15 Td).

Nonuniform power deposition by the e beam in the ion-

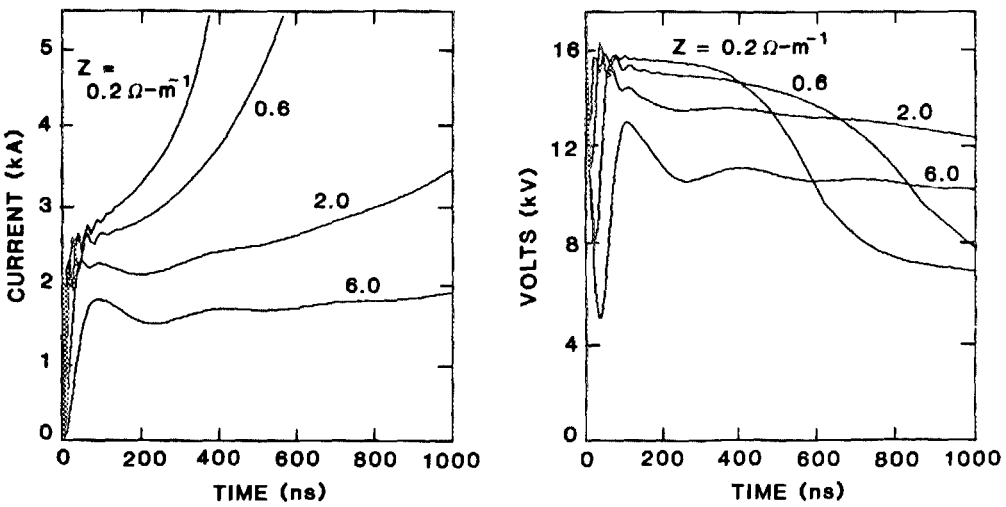

FIG. 8. Current and voltage as a function of time for discharges with PFLs of specified impedance. The charging voltage on the PFL is 16 Td (1 kV = 1 Td). The PFL impedance has units of ohms per unit discharge length (Ω/m) for a square discharge aperture. Discharges with lower-impedance circuits suffer an ionization instability more rapidly because the circuit supplies current quickly enough to keep E/N nearly constant.

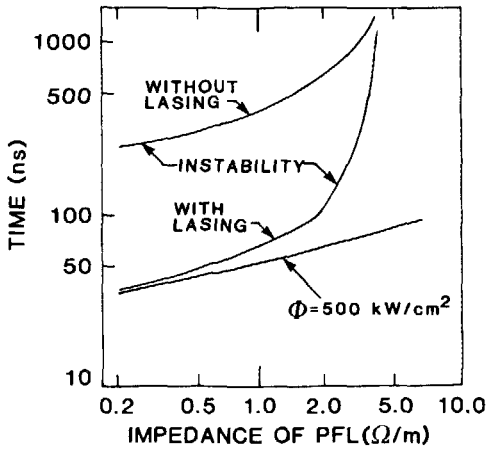

FIG. 9. Time to instability as a function of normalized PFL impedance (Ω/m) for the conditions of Fig. 8. We compare discharges with and without laser oscillation (mirror reflectivity 90%) and also show the time at which the intracavity laser flux crosses 500 kW cm^{-2}. Discharges with higher-impedance PFLs are less prone to instabilities initiated by photodetachment.

gitudinal direction (parallel to the applied electric field) tends to be self-compensating and does not directly lead to an ionization instability. An example of an EBSD where *e* beam power deposition is not uniform in the longitudinal direction appears in Fig. 10. In this and the following figures, the *e* beam is incident through the upper electrode. The plots show values for the shaded region in Fig. 2 and are symmetric across the left plane of the figures. The spatial distribution of *e*-beam power deposition is shown at the left of Fig. 10. The local electric field and the total power deposition (*e* beam plus discharge) are plotted at three successive times during the current pulse. The nonparallel electric field vectors at the right side of the plots result, in part, from edge effects of the electrodes. Note that the total power deposition and electric field are largest near the lower electrode whereas the *e*-beam power deposition is highest near the upper electrode.

The difference in the distribution of total power deposition compared to that for the *e* beam alone results from the *e* beam being more efficient at producing ions (per unit energy deposited) than are the bulk electrons by joule heating (i.e., $j \cdot E$). This is particularly true early during the current pulse when multistep ionization by bulk electrons is not yet important. The disparity in power deposition is explained as follows. The plasma near the top electrode, where *e*-beam power deposition is large, initially has a higher electron density and higher conductivity than near the lower electrode. The local electric field is therefore initially lower near the upper electrode and is proportionally higher near the lower electrode. The larger electric field near the lower electrode is required to equal the rate of ionization of the more efficient *e* beam near the upper electrode and sustain the longitudinal flow of current. As the density of excited states of Ar and Kr, and the efficiency of multistep ionization increase near the lower electrode, the longitudinal distributions of electric field and of power deposition begin to become more uniform.

A similar sequence of plots for total power deposition appears in Fig. 11 where the *e* beam is both longitudinally and transversely nonuniform. Within the first 20–30 ns of the current pulse, power deposition constricts to a narrower transverse profile than that of the *e* beam . This profile then remains nearly stable for the next 200–300 ns or until an ionization instability occurs (see below). The uniformity of power deposition in the longitudinal direction, though, im-

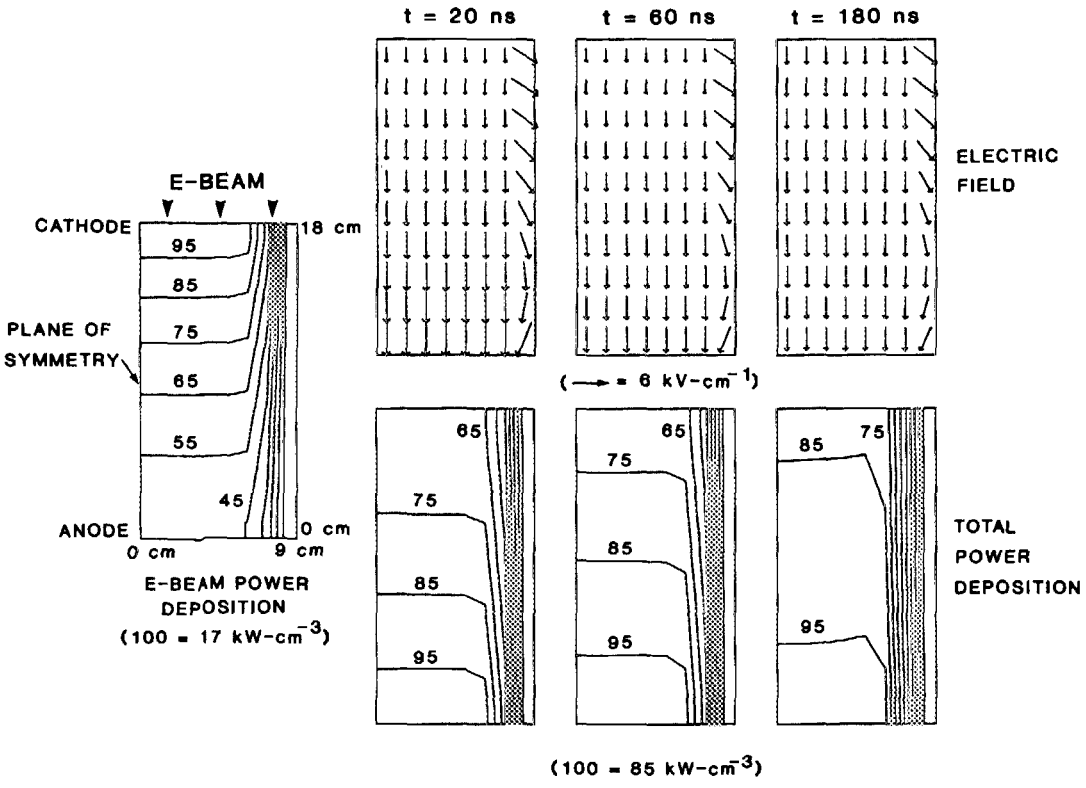

FIG. 10. *e*-beam power deposition, electric field, and total power deposition as a function of position and time for the large aperture discharge. *e*-beam power deposition is nonuniform in the longitudinal direction.

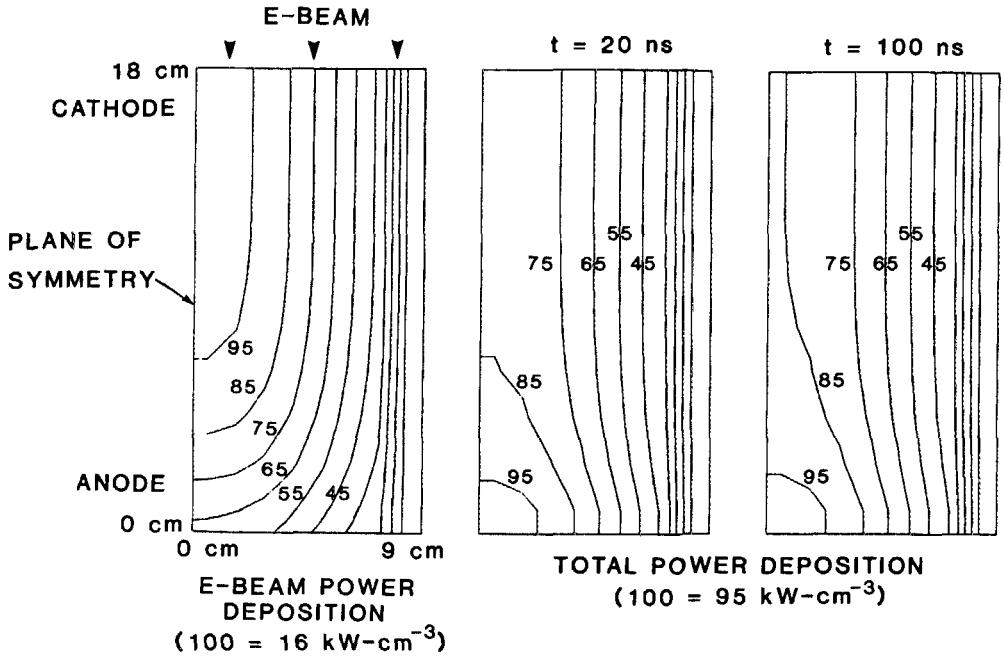

FIG. 11. *e*-beam power deposition and total power deposition as a function of position and time for transversely nonuniform *e*-beam power deposition. Longitudinal power deposition becomes more uniform. Transverse power deposition constricts from the power distribution of the *e* beam.

proves with time as it did in the previous example.

The degree to which the discharge initially constricts in the transverse direction depends upon the transverse uniformity of the sustaining *e* beam . Discharge constriction as a function of uniformity of the *e* beam in the transverse direction is plotted in Fig. 12. The spatially averaged power deposition by the *e* beam is a constant while the transverse profile of the *e* beam is varied. The transverse location of the total power deposition contour corresponding to 65% of the instantaneous maximum value is plotted as a function of time. This transverse location is normalized by the location of the 65% power contour of the *e* beam alone, thereby giving a measure of constriction due to power from the discharge. Results are plotted for discharges with and without laser oscillations. The discharges in Fig. 12 that are not operated as lasers have discharge enhancements of $4.5 \leqslant \eta \leqslant 5.5$ and do not suffer ionization instabilities. The initial fractional constriction of the discharge increases with decreasing uniformity of the *e* beam. For severely nonuniform *e*-beam power deposition, the discharge continues to constrict; for fairly uniform *e*-beam power deposition, a stable transverse configuration is reached after the initial constriction. The degree of constriction increases with increasing η.

When the EBSDs of Fig. 12 are operated as lasers, the degree of constriction significantly increases. The effect is magnified for purposes of illustration by using an output mirror reflectivity of 70% (see Fig. 6). The sudden increase in constriction of the discharge occurs approximately at the time at which the laser reaches threshold, denoted by L_T. Simultaneous to the sudden increase in constriction of the discharges at L_T, the discharge also suffers an ionization instability (See Fig. 13). From these and other results, one can correlate the onset of constriction in an otherwise spatially stable discharge with the onset of an ionization instability. The degree of constriction depends upon the uniformity of the sustaining *e* beam. These results agree well with the experimental observations of Rokni *et al.*[3] and Brown and Nighan.[4]

We have correlated the onset of discharge constriction with the sudden onset of an ionization instability when the *e* beam is not uniform. The converse correlation can also be made. Power deposition by the *e* beam which is not uniform can reduce the time required for an ionization instability to develop. This correlation is shown in Fig. 14 where discharge current is plotted for uniform and nonuniform *e* beam power deposition. The ionization instability is initiated

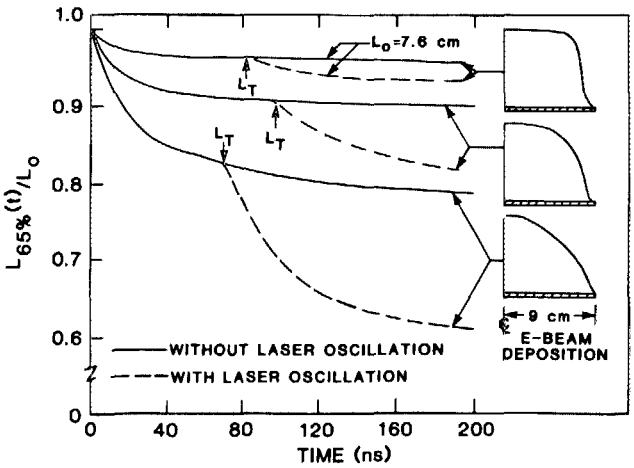

FIG. 12. Discharge constriction as a function of the uniformity of *e*-beam power deposition. The *e*-beam power deposition profiles are shown by the sketches. The value plotted is the distance from the center line of the discharge at which power deposition is 65% that of the instantaneous maximum value divided by the analogous distance for the *e* beam alone. The decrease in this quotient is a measure of the constriction of the discharge. Cases with and without laser oscillation are shown (mirror reflectivity 70%). The onset of laser oscillation denoted L_T initiates an ionization instability which causes further discharge constriction.

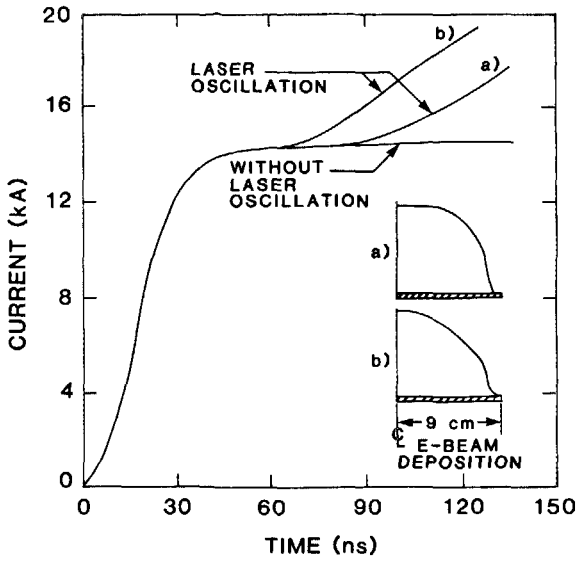

FIG. 13. Discharge current for two cases of nonuniform *e*-beam power deposition from Fig. 12. Without oscillation, discharge current for both examples is nearly identical. The less uniform discharge suffers an ionization instability sooner.

sooner with the nonuniform *e* beam even though the E/N across the discharge is essentially the same as for the uniform case. This is a result of the electron density on the center line of the nonuniform discharge being higher than the average electron density of the uniform discharge thereby leading to a higher rate of excitation of Kr* and Ar*. The increase in the electron density in the constricted region is also sufficiently higher that the electron distribution function becomes more Maxwellian in character. As discussed above, this change in the electron distribution function increases the rate of ionization and excitation, thereby contributing to the instability.

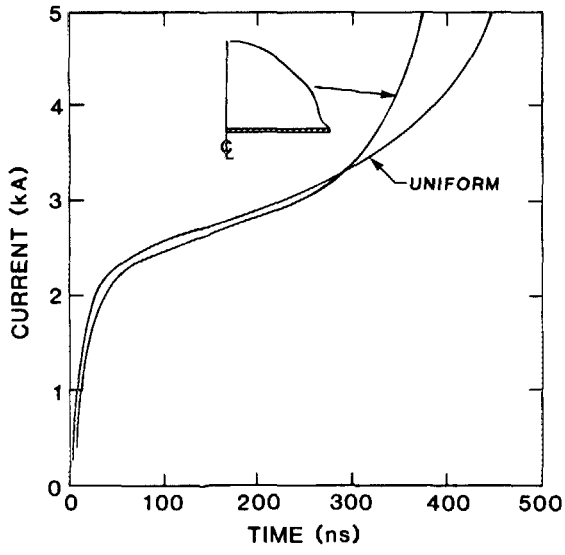

FIG. 14. Current for the small aperture discharge for uniform and nonuniform *e*-beam power deposition. The example with nonuniform power deposition suffers an ionization instability more rapidly.

VI. CONCLUDING REMARKS

The ionization and spatial stability of *e*-beam sustained discharges from KrF excimer lasers have been discussed with results from a two-dimensional, time-dependent discharge and kinetics model. We found that the random flux of UV photons from spontaneous emission of KrF* is sufficient to prematurely initiate an ionization instability. The effect is magnified when operating the discharge as a laser when an ionization instability can be initiated at laser threshold. The onset of ionization instabilities is delayed or eliminated by operating the discharge with electrical PFLs having high impedance per unit discharge length. This stabilizing effect results from limiting the rate of current rise through the discharge. An EBSD that is stabilized against an ionization instability by a high-impedance PFL will nevertheless constrict when sustained by a nonuniform *e* beam. When the *e*-beam power deposition is nonuniform, the time for the onset of an ionization instability is shortened. An EBSD having a nonuniform *e* beam but operating in a spatially stable mode will begin to further constrict upon initiation of an ionization instability.

ACKNOWLEDGMENTS

The authors would like to thank Dr. R. Haas of the University of California (Davis) for discussions on discharge stability and Dr. E. T. Salesky of North-East Research Associates for sharing his preliminary work on EBSD lasers. The authors would also like to thank Dr. D. Hanson, Dr. P. J. Hay, and Dr. R. Berggren of Los Alamos National Lab for their support of this work.

[1] J. D. Daugherty, J. A. Mangano, and J. H. Jacob, Appl. Phys. Lett. **28**, 581 (1976).
[2] J. H. Jacob and J. A. Mangano, Appl. Phys. Lett. **28**, 724 (1976).
[3] M. Rokni, J. A. Mangano, J. H. Jacob, and J. C. Hsia, IEEE J. Quantum Electron. **QE-14**, 464 (1978).
[4] R. T. Brown and W. L. Nighan, Appl. Phys. Lett. **32**, 730 (1978).
[5] W. L. Nighan, IEEE J. Quantum Electron. **QE-14**, 714 (1978).
[6] W. H. Long, J. Appl. Phys. **50**, 168 (1979).
[7] R. T. Brown and W. L. Nighan, Appl. Phys. Lett. **35**, 142 (1979).
[8] R. A. Haas, *Applied Atomic Collisions Physics, Vol. 3: Gas Lasers*, edited by E. W. McDaniel and W. L. Nighan (Academic, New York, 1982), pp. 423–452.
[9] J. Coutts and C. E. Webb, J. Appl. Phys. **59**, 704 (1986).
[10] J. A. Mangano and J. H. Jacob, Appl. Phys. Lett. **27**, 495 (1975).
[11] W. B. Lacina and D. B. Cohn, Appl. Phys. Lett. **32**, 106 (1978).
[12] W. H. Long and R. S. Bradford, IEEE J. Quantum Electron. **QE-15**, 327 (1979).
[13] M. J. Kushner, A. L. Pindroh, C. H. Fisher, T. A. Znotins, and J. J. Ewing, J. Appl. Phys. **57**, 2406 (1985).
[14] W. L. Nighan, Appl. Phys. Lett. **32**, 297 (1978).
[15] W. H. Long, Appl. Phys. Lett. **31**, 391 (1977).
[16] The referenced models are meant to be representative of those reported during the last few years, and not an exhaustive list of all models.
[17] A. E. Green and C. A. Brau, IEEE J. Quantum Electron. **QE-14**, 951 (1978).
[18] T. H. Johnson and A. M. Hunter, J. Appl. Phys. **51**, 2406 (1980).
[19] D. E. Klimek, J. C. Hsia, J. H. Jacob, D. W. Trainor, C. Duzy, and H. A. Hyman, IEEE J. Quantum Electron. **QE-17**, 1847 (1981); **37**, 552 (1980).

[20]W. L. Morgan, N. W. Winter, and K. C. Kulander, J. Appl. Phys. **54**, 4275 (1983).
[21]W. J. Witteman and B. M. H. H. Kleikamp, J. Appl. Phys. **55**, 1299 (1984).
[22]A. Mandl, D. Klimek, and J. H. Parks, J. Appl. Phys. **55**, 3940 (1984).
[23]F. Kannari, M. Obara, and T. Fujioka, J. Appl. Phys. **57**, 4309 (1985).
[24]"New Techniques For KrF Laser Fusion Systems," Spectra Technology, Inc., Final Report Contract No. 9-X65-W1478-1 (1986).
[25]M. Hayashi and T. Nimura, J. Appl. Phys. **54**, 4879 (1983).
[26]W. L. Morgan, "ELENDIF: A Computer Program that Solves the Boltzmann Equation for a Partially Ionized Gas," Joint Institute for Laboratory Astrophysics Report No. 19, University of Colorado (1979).
[27]M. J. Kushner and B. E. Warner, J. Appl. Phys. **54**, 2970 (1983).
[28]W. F. Ames, *Numerical Methods for Partial Differential Equations,* 2nd ed. (Academic, New York, 1977), pp. 114–135.